THE JOURNAL OF PHYSICAL CHEMISTRY C

Article

pubs.acs.org/JPCC

Hydrogen Adsorption Structures and Energetics on Iron Surfaces at High Coverage

Tao Wang,[†] Shengguang Wang,[‡] Qiquan Luo,[†] Yong-Wang Li,[‡] Jianguo Wang,[‡] Matthias Beller,[†] and Haijun Jiao*,[†,‡]

[†]Leibniz-Institut für Katalyse e.V. an der Universität Rostock, Albert-Einstein Straße 29a, 18059 Rostock, Germany

[‡]State Key Laboratory of Coal Conversion, Institute of Coal Chemistry, Chinese Academy of Sciences, Taiyuan, Shanxi 030001, China

Supporting Information

ABSTRACT: Hydrogen adsorption structures and energetics on the (100), (110), (111), (210), (211), (310), and (321) iron surfaces up to saturation have been computed using spin-polarized density functional theory and ab initio thermodynamics. The computed hydrogen desorption temperatures and energies on the (100), (110), (111), and (211) surfaces as well as the Fe−H binding energies on the (110) and (111) surfaces agree well with the available experimental data. At typical hydrogen reduction temperature (675 K), the mainly exposed (110) and (310) facets represent the active surfaces, as supported by the transmission electron microscopy study. Our results offer an example of investigating and understanding surface structures and active facets of heterogeneous catalysts under experimental conditions.

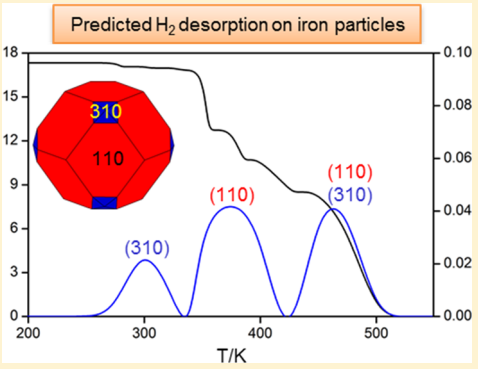

1. INTRODUCTION

Catalysis is a key enabling technology for chemistry, and the world market for catalysts is expected to reach $19.5 billion in 2016.[1] Nowadays, especially heterogeneous catalysts provide the basis for economically and ecologically improved processes for value-added fine and bulk chemicals as well as life science products.[2] In heterogeneous catalysis, the surface active sites are responsible for the specific activity. However, the absence of precise tools for direct characterization and identification of surface active sites has hindered the rational development of heterogeneous catalysts.[3,4] Despite the past significant improvements,[5−7] the available experimental characterization techniques, e.g., X-ray diffraction (XRD), extended X-ray absorption fine structure (EXAFS), X-ray absorption near edge structure (XANES), low-energy electron diffraction (LEED), ultraviolet photoelectron spectroscopy (UPS), transmission electron microscopy (TEM), scanning transmission electron microscopy (STEM), high-resolution transmission electron microscopy (HRTEM), and scanning tunneling microscopy (STM), cannot yet give the full structural information of real catalysts under working conditions. Hence, identification of individual facets of polycrystalline (or amorphous) materials and rationalization of different catalytic properties of catalysts prepared from the same starting materials but by different methods are not easily possible by using experimental approaches. In investigations of catalytic surface adsorption phenomena and activities, temperature-programmed techniques (TPX) provide useful information about solid surfaces,[8] adsorption properties of gas species, and thermal stability of adsorption states, but TPX can give only indirect information and cannot identify and differentiate individual active sites.

Iron-based heterogeneous catalysts are widely applied in industry. For example, ammonia[9] and Fischer−Tropsch syntheses[10,11] are two of the most important large-scale industrial processes, where hydrogen is used as the principal reactant. Hence, investigating hydrogen adsorption on the surface of iron particles provides an ideal example for understanding structure and reactivity relationships in heterogeneous catalysis. Despite the significant industrial importance of hydrogen interaction with iron surfaces, few systematic experimental and theoretical studies about this system have been reported. Experimentally, Bozso et al.[12] studied hydrogen chemisorption on iron (100), (110), and (111) surfaces by applying LEED, thermal desorption spectroscopy (TDS), UPS, and work-function measurement under UHV conditions and provided the adsorption as well as desorption properties of hydrogen on these surfaces. Equilibration and exchange reaction between H_2 and D_2 on polycrystalline films as well as on the iron (100), (110), and (111) surfaces[13] indicate that hydrogen adsorbs dissociatively. Dissociative hydrogen adsorption was also found by Yoshida et al.[14] in their studies about the chemisorption of CO, CO_2, C, C_2H_4, H_2, and NH_3 on clean iron (100) and (111) surfaces. The ordered overlayer structures were found by Imbihl et al.[15] in their LEED studies about the

Received: October 28, 2013
Revised: February 5, 2014
Published: February 5, 2014

dx.doi.org/10.1021/jp410635z | J. Phys. Chem. C 2014, 118, 4181−4188

interaction of hydrogen with the Fe(110) surface. Nichtl-Pecher et al.[16] reported a LEED study of hydrogen adsorption on the Fe(110) surface and found a new 2 × 2-2H superstructure which reversibly transforms to the $c(2 \times 2)$ phase at about 80 K. Schmiedl et al.[17] reported a LEED and TDS study of the interaction of hydrogen with the Fe(211) surface and found the metastable commensurate phase at temperatures less than 200 K and the reconstructed phases at temperatures greater than 200 K. Schmiedl et al.[18] further studied the structural, thermodynamic, and kinetic properties of hydrogen on the Fe(211) surface by using LEED, TDS, and work-function measurement and found that the activation barrier for the transition from the commensurate phase to reconstructed phase is 0.34 ± 0.04 eV and hydrogen desorption energy is 1.05 ± 0.02 eV. High-resolution electron energy loss spectroscopy (HREELS) measurements[19] reveal that hydrogen prefers the 4-fold hollow site on the Fe(100) surface. Suo et al.[20] reported two peaks of hydrogen desorption at about 350 and 425 K on the supported iron catalyst in their studies about the chemical and structural effects of silica in iron-based Fischer−Tropsch synthesis catalysts.

Compared with extensive experimental studies about the interaction of hydrogen with iron, few theoretical calculations are known. Early Hartree−Fock calculations using cluster models by Walch[21] reveal that H prefers the 4-fold hollow site on the Fe(100) surface. Sorescu[22] systematically studied the adsorption and diffusion of hydrogen on the Fe(100) surface by using DFT calculations and found that the site preference depends on hydrogen coverage and that H diffusion from surface to subsurface is more difficult than on the surface. van Steen[23] reported a DFT study about H_2 dissociation on CO and C precovered Fe(100) surface and hydrogen dissociation is found to be blocked by CO and C adsorption. Jiang et al.[24] present a DFT study about the interaction of hydrogen with the Fe(110) surface as a function of coverage and found H to prefer the 3-fold site. Jiang et al.[25] also reported a periodic spin-polarized DFT calculation of hydrogen adsorption, absorption, and dissolution as well as diffusion on and in bcc iron and found that H prefers to stay on the Fe surface instead of subsurfaces or in bulk. Huo et al.[26] performed a spin-polarized DFT calculation to characterize the adsorption and diffusion of hydrogen on the Fe(111) surface and found the top-shallow bridge site to be most favored. Fabiani[27] studied the adsorption properties of hydrogen on the Fe(310) surface by using DFT calculations and compared those on the Fe(100) surface. It revealed that the site preference of hydrogen is different on these two surfaces despite their similar structures. Faglioni et al.[28] reported a systematic DFT study about the coverage-dependent hydrogen adsorption on the closest packed surface of all nine group VIII transition metals (including Fe(110) and Fe(111)), leading to results consistent with the available surface science studies. On the basis of these results, they also developed a simple thermodynamic model useful in estimating the surface coverage under typical heterogeneous catalysis conditions.

For several decades a major goal in catalysis research has been the rational development of state of the art materials. To achieve this goal, not only specific experimental characterization tools but also high-level DFT computations might play a complementary and decisive role.[29] Commonly, DFT computations describe the structures and properties of materials at atomic scales. Ideally, interplay of informative experimental techniques and accurate DFT computations can synergistically provide insights into surface structures of catalysts and rationalize the catalytic activities and in turn facilitate the rational design of novel selective catalysts.[30] On the basis of experimental studies of hydrogen adsorption on several iron single crystal surfaces, we carried out systematic DFT computations on the surface morphology of Fe particles and hydrogen adsorption properties on seven iron surfaces from ab initio thermodynamics.[31,32] Our goal is to characterize and identify the possible active facets of Fe particles from the computed hydrogen adsorption properties on single-crystal surfaces in combination with the experimental temperature-programmed desorption (TPD) data.

2. COMPUTATIONAL DETAILS

2.1. Method and Models. All spin-polarized periodic DFT calculations were carried out using the Perdew−Burke−Ernzerhof (PBE) functional[33] and projector augmented wave potential (PAW)[34,35] as implemented in VASP code.[36,37] Spin polarization was included for iron systems to correctly account for its magnetic properties, and this was found to be essential for an accurate description of adsorption energy.[38] An energy cutoff of 400 eV and a second-order Methfessel−Paxton[39] electron smearing with $\sigma = 0.2$ eV were used to ensure accurate energies with errors less than 1 meV per atom. The geometry optimization was done when forces became smaller than 0.02 eV/Å and the energy difference was lower than 10^{-4} eV. Calculations on α-Fe bulk crystal structure with a k-point mesh of 9 × 9 × 9 give a lattice constant of 2.84 Å and a local spin magnetic moment of 2.214 μ_B, in good agreement with other DFT calculations[40,41] and experiment.[42] For studying hydrogen adsorption, the $p(3 \times 4)$, $p(4 \times 4)$, $p(3 \times 3)$, $p(3 \times 2)$, $p(4 \times 2)$, $p(3 \times 2)$, and $p(2 \times 3)$ super cells were used for the (100), (110), (111), (210), (211), (310), and (321) surfaces, respectively. The 3 × 3 × 1 Monkhorst−Pack k-point grid was used in all the surfaces for sampling the Brillouin zone. The vacuum layer between periodically repeated slabs was set as 12 Å to avoid interactions between slabs. All reported stable adsorption configurations were verified to be energy minima by frequency analysis.

2.2. Ab Initio Thermodynamics. As a convenient tool to solve problems referring to real reaction conditions, atomistic thermodynamics proposed by Scheffler and Reuter have been widely and successfully applied in many systems.[43−50] In this method, the surface free energy γ of a surface can be described as in eq 1, in which G is the Gibbs free energy of a solid surface, A the total surface area of two equilibrium surfaces (top and bottom sides), $\mu_i(T, p)$ the chemical potential of the species i, and n_i the number of the ith type species.

$$\gamma(T, p) = \frac{1}{A}[G - \sum_i n_i \mu_i(T, p)] \quad (1)$$

For describing the adsorption of gas species on surfaces, we define the surface energy of a surface with n_i gas species adsorption as in eq 2, where $G^{ads}_{hkl}(T,p,\{n^{ads}_{gas}\})$is the Gibbs free energy of the (hkl) surface with n adsorbed species and μ_i(T, p) is the chemical potential of all the species in the system (including the adsorbed species).

$$\gamma^{ads}_{hkl}(T, p, n_i) = \frac{1}{A}[G^{ads}_{hkl}(T, p, \{n^{ads}_{gas}\}) - \sum_i n_i \mu_i(T, p)] \quad (2)$$

dx.doi.org/10.1021/jp410635z | J. Phys. Chem. C 2014, 118, 4181−4188

For iron surfaces with nH atoms adsorption, eq 2 can be rewritten as

$$\gamma_{Fe}^{ads}(T, p, nH) = \frac{1}{A}\left[G_{Fe}^{ads}(T, p, \{nH\}) - n_{Fe}\mu_{Fe}(T, p) - \frac{1}{2}n_H\mu_{H_2}(T, p)\right] \quad (3)$$

As for the clean iron surfaces, the surface free energy ($\gamma_{Fe}^{clean}(T, p)$) is given in eq 4:

$$\gamma_{Fe}^{clean}(T, p) = \frac{1}{A}[G_{Fe}^{clean}(T, p) - n_{Fe}\mu_{Fe}(T, p)] \quad (4)$$

where $G_{Fe}^{clean}(T, p)$ represents the Gibbs free energy of the clean Fe surface and $\mu_{Fe}(T, p)$ is the chemical potential of bulk Fe. The surface free energy of the (hkl) surface with n H atoms by inserting eq 4 to eq 3 is given in eq 5.

$$\gamma_{Fe}^{ads}(T, p, nH) = \gamma_{Fe}^{clean}(T, p) + \frac{1}{A}\left[G_{Fe}^{ads}(T, p, \{nH\}) - G_{Fe}^{clean}(T, p) - \frac{1}{2}n_H\mu_{H_2}(T, p)\right] \quad (5)$$

Considering the adsorption process of H atoms on Fe surface as

$$Fe(hkl) + nH \leftrightarrow Fe(hkl)/\{nH\}$$

the change of Gibbs free energy for those adsorption processes, $\Delta G_{Fe}^{ads}(T,p,nH)$, can be found in eq 6.

$$\Delta G_{Fe}^{ads}(T, p, nH) = G[Fe(hkl)/\{nH\}] - G[Fe(hkl)] - \frac{1}{2}G_{gas}(H_2) \quad (6)$$

In this equation, $G[Fe(hkl)/\{nH\}]$ is the Gibbs free energy of an Fe surface with nH atoms, while $G[Fe(hkl)]$ is the Gibbs free energy of the clean Fe surface. Compared with the large contribution of vibration to the gases, this contribution to the solid surfaces is negligible because of their large mass differences. Therefore, we apply the DFT-calculated total energy to substitute the Gibbs free energies of solid Fe surfaces, and eq 6 can be rewritten as

$$\Delta G_{Fe}^{ads}(T, p, nH) = E[Fe(hkl)/\{nH\}] - E[Fe(hkl)] - \frac{1}{2}G_{gas}(H_2)$$

where $E[Fe(hkl)/\{nH\}]$ and $E[Fe(hkl)]$ are the total energies of corresponding systems. The $G_{gas}(H_2)$ term equals $n\mu_{H_2}(T, p)$. Then, the chemical potential of $H_2(\mu_{H_2})$ can be described as

$$\mu_{H_2}(T, p) = E_{H_2}^{total} + \tilde{\mu}_{H_2}(T, p^0) + k_BT\ln\frac{p_{H_2}}{p^0}$$

At 0 K, the chemical potential of H_2 can be regarded as the total energy of an isolated H_2 molecule, which can be calculated directly with VASP. The $\tilde{\mu}_{H_2}(T, p^0)$ term includes the contributions from vibration and rotation of the H_2 molecule. It can be calculated or found in thermodynamic tables. In this paper we calculate these data by Gaussian software.[51] The last term of the formula is the contributions of temperature and H_2 partial pressure to the chemical potential. Finally, the change in the Gibbs free energy of the Fe surfaces after the adsorption of n H atoms can be expressed as

$$\Delta G_{Fe}^{ads}(T, p, nH) = E[Fe(hkl)/\{nH\}] - E[Fe(hkl)] - \frac{1}{2}nE_{H_2}^{total} - \frac{1}{2}n\tilde{\mu}_{H_2}(T, p^0) - \frac{1}{2}nk_BT\ln\frac{p_{H_2}}{p^0} \quad (7)$$

In this respect, we can plot $\Delta G(T, p)$ as a function of T and p. The system (surface with nH atoms adsorption) with the lowest value of $\Delta G(T, p)$ will be most stable under the given conditions, and this also provides information about the H_2 equilibrium coverage on the Fe surface under fixed conditions. Furthermore, the $\Delta G_{Fe}^{ads}(T, p, nH)$ part is equal to the second part of eq 5. Finally, we can get the value of the surface free energy of a surface with nH atoms adsorption under different temperatures and pressures by adding the contribution of hydrogen adsorption by using eq 8.

$$\gamma_{Fe}^{ads}(T, p, nH) = \gamma_{Fe}^{clean}(T, p) + \frac{1}{A}[\Delta G_{Fe}^{ads}(T, p, \{nH\})] \quad (8)$$

The surface energy of clean iron surface (γFe) can be written as

$$\gamma_{Fe}^{clean}(T, p) = \frac{1}{A}[E_{Fe(hkl)} - n_{Fe}E_{Fe\text{-}bulk}] \quad (9)$$

where $E_{Fe(hkl)}$ is the total energy of $Fe(hkl)$ surface and $E_{Fe\text{-}bulk}$ is the total energy of bulk iron.

3. RESULTS AND DISCUSSION

3.1. Surface Structures and Hydrogen Adsorption.

The morphology of real catalysts plays a key role in heterogeneous catalysis, and it is possible to get a clear picture of a practical catalyst only by considering all possible structures. For Fe particles, the seven body-centered cubic iron surfaces were considered, i.e., low index (100), (110), and (111) surfaces for the basic structures and high index (210), (211), (310), and (321) surfaces for the step and kinked structures (Figure 1).

For obtaining the most stable adsorption sites at any coverage, all adsorption sites and configurations were calculated. To determine the saturated coverage on a specific surface, the stepwise adsorption energy, $\Delta E_{ads} = E[H_{n+1}/slab] - E[H_n/slab] - 1/2E[H_2]$, was used, where a positive ΔE_{ads}

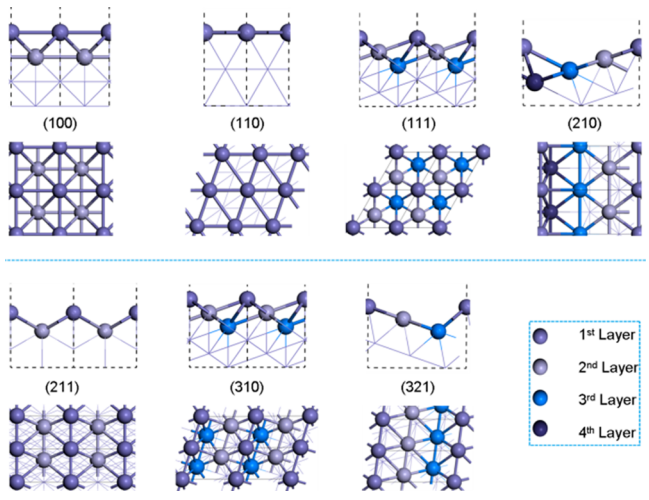

Figure 1. Schematic side and top views of seven iron surfaces (larger sizes are used in calculations).

dx.doi.org/10.1021/jp410635z | J. Phys. Chem. C 2014, 118, 4181−4188

indicates the saturated adsorption with hydrogen atoms on the surface. It is worth noting that our stepwise adsorption energy defines the change of the adsorption energy by adding one more species to the surface, whereas the differential energy of adsorption defines the change of the average adsorption energy per coverage as the function of coverage.[52] The binding energy (E_b) is defined as the adsorption energy of one H atom. All our reported energetics includes the correction of zero-point energy (ZPE) between the adsorbed surface H atoms and H_2 in the gas phase. As shown in Supporting Information (Table S1), ZPE correction has a maximal effect of only 0.7 kcal/mol (or 0.03 eV) to the binding energies on all surfaces. The contribution of ZPE correction to the stepwise adsorption energies on all seven surfaces (Tables S2−S8 of Supporting Information) has maximal absolute effect of 1.15 kcal/mol (or 0.05 eV). In our calculations, we observed only dissociative hydrogen adsorption up to saturation on all surfaces, in agreement with the experimental results. The structures of the most stable sites for hydrogen atom stepwise adsorption on these surfaces are given in Supporting Information (Figures S1−S7).

3.2. Gibbs Free Energy with Temperature and Pressure. On the basis of the saturated coverage determined by ΔE_{ads}, we want to connect stable hydrogen coverage with experimental conditions (temperature and pressure) by using Gibbs free energy as the criterion. Figure 2 presents the

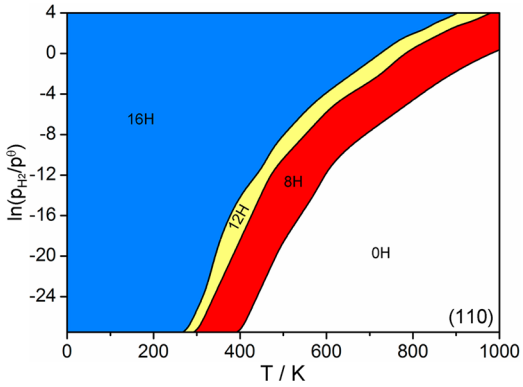

Figure 2. Equilibrium phase diagram of H coverage on the (110) surface.

relationship between the stable H coverage with temperatures and hydrogen partial pressure on the Fe(110) surface. It indicates clearly that the stable hydrogen coverage decreases upon temperature increase at given pressures. On the basis of the equilibrium phase diagram of hydrogen coverage, one can directly get the stable hydrogen coverage under any given T and p_{H_2}. The phase diagrams of the other six surfaces are given in Supporting Information (Figure S8). Systematic comparisons reveal that each surface has quite different hydrogen coverage even under the same conditions, which rationalizes the experimentally observed differences in activities of catalysts prepared under different conditions.

3.3. Morphology of Iron Particles under Different Conditions. Because Fe particles are usually prepared experimentally from Fe_2O_3 and H_2, the reduction conditions play important roles in the formation of Fe surface morphology. On the basis of surface free energy of the iron surfaces (Tables S9 and S10 in Supporting Information), we modeled the iron crystal shapes at different temperatures and one atmosphere hydrogen pressure using Wulff constructions.[53,54] In addition, those crystal shapes resulting at 675 K reduction temperature and different hydrogen pressures are given in Supporting Information (Figure S9). Because the reduction conditions affect the surface morphology of Fe particles, we chose four temperatures to discuss the change in morphology of the Fe particles. Under ideal conditions, the morphology of iron particles is polycrystalline (Figure 3a). Under hydrogen

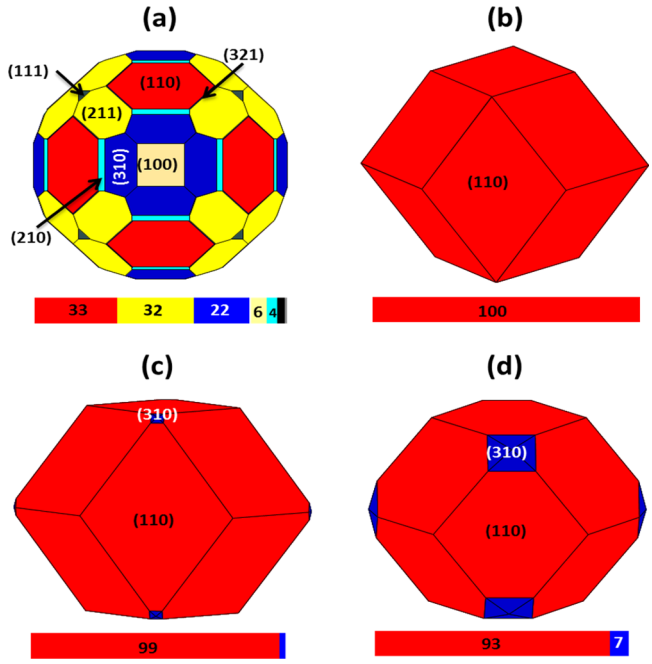

Figure 3. Wulff shapes of clean iron particles at 0 K under vacuum (a) and iron particles under hydrogen atmosphere at (b) 0 K, (c) 425 K, and (d) 675 K.

atmosphere at 0 K, the only exposed surface is (110) (Figure 3b). At 425 K (low reduction temperature), the (310) surface starts to expose apart from the (110) surface (Figure 3c). At 675 K (common reduction temperature), the portion of the (310) surface increases, but the (110) surface still dominates (Figure 3d). These results are in agreement with the recent TEM analysis on Fe particles reduced at 673 K for 30 h under pure H_2.[55] Our analysis shows that the Fe(110) surface is most stable under hydrogen reduction and should be expected to be least active. Indeed, the Fe(110) surface has been proven to have the lowest activity in ammonia synthesis compared to the Fe(100) and Fe(111) surfaces.[56]

3.4. Hydrogen Adsorption and Desorption Properties on Iron Surfaces. Because the experimentally synthesized catalyst particles are always polycrystalline with mixed facets and an unambiguous determination of their three-dimensional atomic-scale structures is challenging,[57,58] a clear identification and characterization of the surface active sites is desired. Here, we present the full portrait of Fe particles from the computed hydrogen desorption temperatures and energies on single-crystalline iron surfaces in combination with the experimental TPD results to identify and differentiate the surface active sites.

The equilibrium adsorption configurations depend on coverage and temperature and are dominated by the mutual interactions of adsorbed surface species. Because hydrogen coverage decreases with increasing temperature, each desorption peak at a certain temperature shows the corresponding sharp and sudden change of the equilibrium coverage. On the

dx.doi.org/10.1021/jp410635z | J. Phys. Chem. C 2014, 118, 4181−4188

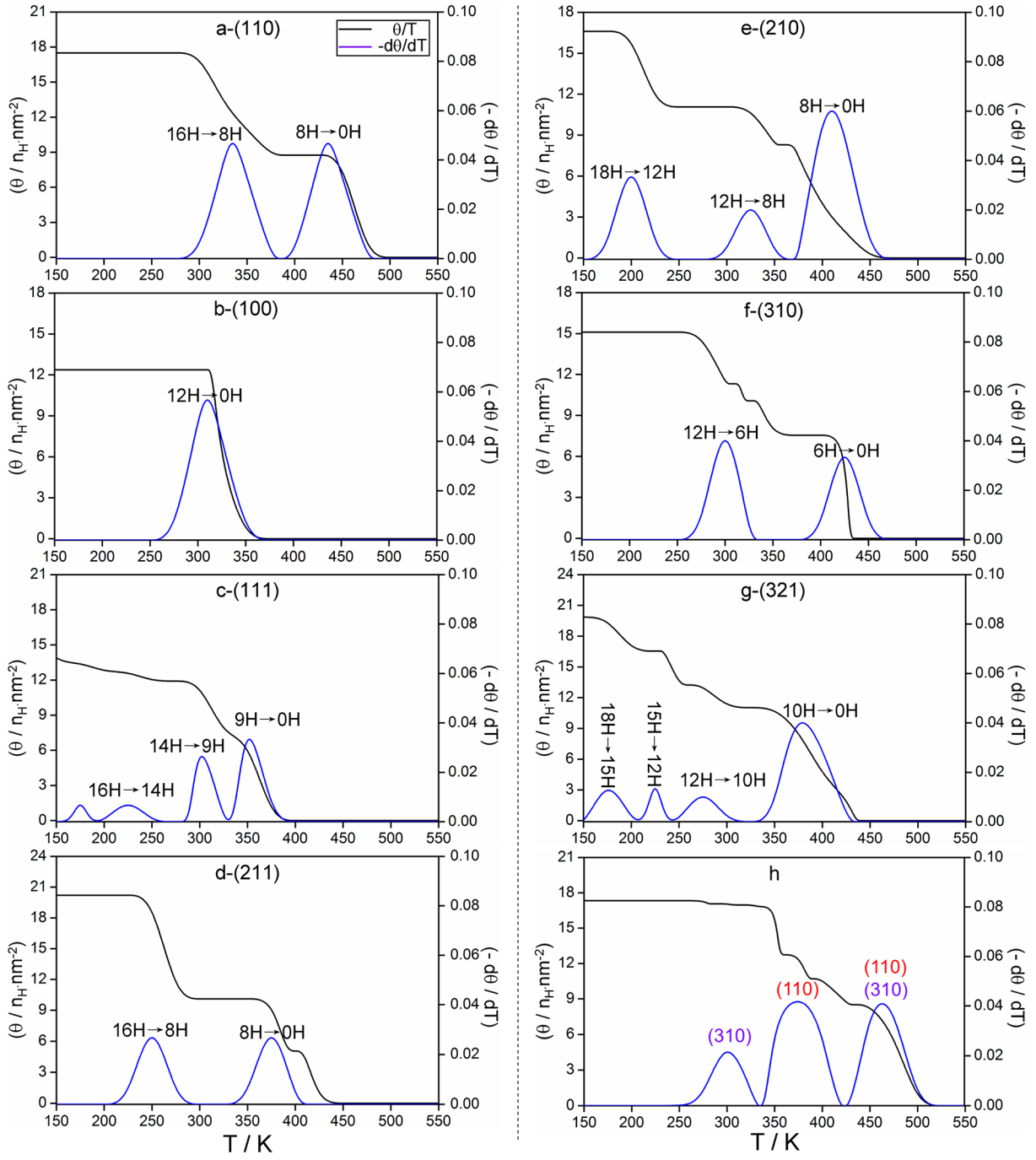

Figure 4. Hydrogen desorption peaks (blue curve) on seven iron surfaces at 10^{-9} atmosphere (a–g) as well as hydrogen desorption peaks on iron particles prepared at 675 K and hydrogen atmosphere pressure (h).

basis of the changes in Gibbs free energies of hydrogen adsorption at different temperatures, the changes in hydrogen coverage on seven iron surfaces at different hydrogen pressures can be obtained. Our results from ultralow (10^{-12} atm) to very high (40 atm) hydrogen pressure show that rising working pressure increases the desorption temperature. Because the available TPD spectra on single iron surfaces were carried out under ultrahigh vacuum (UHV) conditions and different exposures, we used the data at 10^{-9} atm (1 L = 10^{-6} Torr/s means keeping the pressure of hydrogen gas at 10^{-6} Torr for one second; in this respect, the partial pressure of H_2 is 10^{-6} Torr, which is equal to 10^{-9} atm) starting from the saturated coverage for discussion and comparison (Figure 4).

Hydrogen adsorption on the (110), (100), and (111) single crystal planes after H_2 exposures has been studied by using TPD, LEED, UPS, and work function measurements by Bozso et al.[12] On Fe(110), the TPD spectra were recorded with a heating rate of 7 K/sec after H_2 exposures between 0.4 and 3500 L at 140 K. The saturation of the adsorbed layer (1 ML) was formed under the highest exposure. The spectra show two states (β_1 and β_2) in superposition. The temperature maximum of the β_1 state is about 340 K, whereas the β_2 state shifts toward higher temperature (480–430 K) with increasing coverage. Analysis into the total desorption area shows that at saturation of the adsorbed layer both states exist with equal hydrogen concentration on the surface.

dx.doi.org/10.1021/jp410635z | J. Phys. Chem. C 2014, 118, 4181–4188

These thermal desorption data are excellently reproduced in our calculations. On Fe(110), for example, the totally saturated coverage of 16H atoms (1 ML for $p(4 \times 4)$ unit cell) is stable up to 250 K (Figure 4a). Two desorption peaks are predicated; the first one has a temperature maximum at about 330 K (300−375 K), and the second one has a temperature maximum at about 425 K (400−450 K). The first desorption loses half of the 16 H atoms at saturation (16 H → 8 H), and the second desorption loses all other adsorbed H atoms (8 H → 0 H), indicating the equal concentration of two states. Detailed analysis into the surface structures shows that all adsorbed H atoms in the 3-fold adsorption configuration are fully equivalent and form the ordered "$c(4 \times 4)$-8H" and "$c(4 \times 4)$-16H" surface structures at both 0.5 and 1.0 ML, respectively, in agreement with those from LEED anaylsis.[12] Up to 8 H atoms (0.5 ML), the stepwise adsorption energies are nearly the same, indicating non repulsive lateral interaction. From 9 H to 16 H atoms (1.0 ML), the stepwise adsorption energies are also nearly the same, but lower than those for 8 H atoms, indicating the repulsive interaction of the neighboring hydrogen atoms as coverage increase. All these are in agreement with the experimental findings. Furthermore, the calculated Fe−H binding energy of 67.5 kcal/mol also agrees with the value (65 kcal/mol) from UPS.[12]

On Fe(100), Bozso et al.[12] found two discernible states (β_1 and β_2). The temperature maximum of the β_1 state is about 300 K, whereas the β_2 state shifts toward higher temperature (430−400 K) with increasing coverage. There are no ordered surface structures over the whole range of coverage from LEED analysis. In our calculation we found one broad desorption state with temperature maximum at about 310 K (Figure 4b), which is very close to the experimentally detected β_1 state. However, we could not find the corresponding temperature maximum of the β_2 state. At about 350 K, all 12 H atoms desorb fully. At 1 ML, all 12 H atoms are fully equivalent and have the 4-fold hollow adsorption configuration. As given in Supporting Information (Figure S10), the saturated coverage on the (100) surface has 13 H, and the first desorption temperature at 50 K is below the exposure temperature (140 K). The computed Fe−H bonding energy is 62.5 kcal/mol.

On Fe(111), Bozso et al.[12] found three desorption states (β_1, β_2, and β_3) in the range of 200−450 K. The temperature maximum of the β_1 and β_2 states is about 240 and 310 K, respectively, whereas the β_3 state shifts toward higher temperature (375−400 K) with increasing coverage. There are no ordered surface structures over the whole range of coverage from LEED analysis. Above 200 K, we also found three desorption states, and the corresponding temperature maxima are 225, 300, and 350 K (Figure 4c), respectively, and these are very close to the experimentally detected β_1, β_2, and β_3 states. The first state indicates the coverage change from 16 H to 14 H and the second state indicates the coverage change from 14 H to 9 H. The third state indicates the full desorption. As given in Supporting Information (Figure S10), the saturated coverage on the Fe(111) surface has 23 H and a broad desorption peak with a temperature maximum at 75−100 K, which is below the exposure temperature (140 K). In addition, the calculated Fe−H binding energy (63.8 kcal/mol) agrees also with the value (62 kcal/mol) from UPS.[12]

On the (211) surface[17] there are unreconstructed and reconstructed surfaces induced by hydrogen at different exposures. On the unreconstructed surface at low exposure temperature (40 K), there are two desorption states: a weaker one (α_1, α_2, and α_3) with a temperature maximum at 250 K and a stronger one (β) with a temperature maximum at about 350 K. Our calculations (Figure 4d) also show two desorption states, i.e., at 250 K for the coverage change from 16 H (saturated, 2 ML) to 8 H (1 ML) and at 375 K for the full desorption of the 8 H atoms. The computed zigzag (1 ML) and linear (2 ML) arrangements of the adsorbed H atoms (Figure S11 of Supporting Information) are supported by ordered surface structures deduced from LEED analysis.[17] In addition, the calculated Fe−H binding energy is 65.3 kcal/mol.

Not only desorption temperatures but also the corresponding desorption energies (details in Supporting Information) have been well-reproduced computationally (Table 1). The excellent agreement in hydrogen desorption temperatures and energies on the (100), (110), (111), and (211) surfaces as well as the H binding energies on the (110) and (111) surfaces between experiments and theory validates this computational methodology and rationalizes the results. Moreover, the computed desorption temperatures and energies on those surfaces (Figure 4e−g) allow the prediction of the hydrogen TPD data on other surfaces, e.g., (210), (310), and (321), which are experimentally not yet available. In addition, all three surfaces have practically the same Fe−H binding energies. Indeed, a recent TPD and DFT study by van Helden et al.[59] reported desorption properties of hydrogen on different Co surfaces and also showed the reasonable agreement between computation and experiment.

Table 1. Binding Energies (E_b), Desorption Energies (E_d), and Desorption Temperature (T) from Computation (Including Zero-Point Energies) and Experiments

surface	E_b[a]	E_d (T)[a] (kcal/mol (K))	E_d (T)[c] (kcal/mol (K))
(110)	67.5 (65)[b]	23.7 (330)	24 (β_1, 340)[12]
		28.3 (425)	26 (β_2, 430−480)[12]
(100)	62.5	17.9 (310)	18 (β_1, 300)[12]
(111)	63.8 (62)[b]	15.3 (225)	13 (β_1, 240)[12]
		17.1 (300)	18 (β_2, 310)[12]
		17.8 (350)	21 (β_3, 375−400)[12]
(211)	65.3	18.9 (250)	9−12 (α_{1-3}, 210−270)
		22.1 (350)	19.6−24.2 (β, 350)[18]
(210)	66.7	19.0 (400)	
(310)	66.6	21.7 (425)	
(321)	66.7	18.4 (400)	

[a]Computed data in this work. [b]UPS data from ref 12. [c]Experimental data.

It is worth noting that our methods can be used to model the adsorption and desorption properties not only under UHV conditions but also under practical operations at high temperature and pressure. At high pressure, the adsorption patterns become different and desorption temperatures become higher. Furthermore, our predicted TPD peaks represent the changes of the most stable surface coverage at a given temperature; those from the framework of the Polanyi−Wigner equations show the maximal rates of desorption. Both approaches are related by desorption energies at given coverage and conditions.

3.5. Revealing the Exposed Surfaces of a Crystalline Catalyst. When our approach is followed, it becomes possible to evaluate and identify surface characteristics by a direct comparison between experimentally detected desorption

dx.doi.org/10.1021/jp410635z | J. Phys. Chem. C 2014, 118, 4181−4188

temperatures and energies on the whole particles and the theoretically computed desorption temperatures and energies on individual clean surfaces (each surface has its characteristic desorption peaks which play the role of the fingerprint of the surface) at the same conditions. Hence, one can obtain the whole portrait as well as the exposed surfaces of the prepared catalysts in a straightforward manner.

As an example, a metallic iron catalyst prepared at 675 K under hydrogen atmosphere (Figure 4h), which is related to ammonia synthesis, shows three desorption peaks. Each one corresponds to an adsorption state on the characteristic surface. Our detailed analysis indicates that this Fe catalyst has the exposed (110) and (310) surfaces. On the basis of the individual desorption peaks on the clean (110) and (310) surface (Figure 4a and 4f), desorption peaks at about 300 K can be assigned to that on the (310) surface and the desorption peak at 350−375 K should belong to the (110) surface. The third peak at about 470 K is a result of the overlap of desorption on both (110) and (310) surfaces. The changes in desorption temperatures and energies clearly reflect the changes in exposed facets and in hydrogen coverage, and they reveal the relationship between the different facets of Fe particles and their properties in hydrogen adsorption or desorption. More specifically, the obtained results make clear that in ammonia synthesis the active catalyst site should be the most exposed (110) surface because of its high surface exposure (93%).

4. CONCLUSION

We computed the surface morphology of Fe particles using ab initio thermodynamics. Notably, the experimentally detected hydrogen desorption temperatures and energies on the (100), (110), (111), and (211) surfaces as well as the Fe−H binding energies on (110) and (111) surfaces are well-reproduced. A precise identification of the structure of the active surface centers and amount of hydrogen atoms on the different surfaces at different temperatures provides the basis for micro kinetic modeling[60] of hydro-treating reactions. Such agreements between theory and experiment validate our computational methodology and reveal that commonly prepared Fe catalysts have exposed (110) and (310) facets at typical hydrogen reduction temperature. This interplay of hydrogen TPD between theory and experiment provides a novel characterization tool for investigating surface structures and active facets of catalyst systems. In addition, it will help to reveal the relationship of surface structures and catalyst activities in general and might thereby contribute to a more rational catalyst development in the future.

■ ASSOCIATED CONTENT

Supporting Information

Detailed desorption of energy calculation methods; effects of zero-point energies on binding and desorption energies (Table S1); stepwise H adsorption energies with and without zero-point energy corrections (Tables S2−S8); surface free energy of seven iron surfaces under different condition (Tables S9 and S10); stepwise H adsorption structures (Figures S1−S7); H equilibrium coverage phase diagrams for all iron surfaces (Figure S8); Wulff shapes of iron particles at different pressures (Figure S9); Hydrogen desorption peaks on seven iron surfaces at 10^{-9} atm (Figure S10); structures of ordered hydrogen adsorption on Fe(110) and (211) surfaces (Figure S11). This material is available free of charge via the Internet at http://pubs.acs.org.

■ AUTHOR INFORMATION

Corresponding Author

*E-mail: haijun.jiao@catalysis.de.

Notes

The authors declare no competing financial interest.

■ ACKNOWLEDGMENTS

This work was supported by the National Basic Research Program of China (2011CB201406), National Natural Science Foundation of China (21073218), Chinese Academy of Sciences and Synfuels CHINA. Co., Ltd. We also acknowledge general financial support from the BMBF and the state of Mecklenburg-Western Pommerania.

■ REFERENCES

(1) http://www.freedoniagroup.com/World-Catalysts.html.

(2) Ertl, G.; Knözinger, H.; Schüth, F.; Weitkamp, J. *Handbook of Heterogeneous Catalysis*, 2nd ed; VCH: Weinheim, Germany, 2008.

(3) Thomas, J. M.; Thomas, W. J. *Principles and Practice of Heterogeneous Catalysis*; Wiley-VCH: Weinheim, Germany, 1997.

(4) Somorjai, G. A.; Li, Y. *Introduction to Surface Chemistry and Catalysis*, 2nd ed.; John Wiley: Hoboken, NJ, 2010.

(5) Somorgai, G. A.; Park, J. Y. Evolution of the Surface Science of Catalysis from Single Crystals to Metal Nanoparticles under Pressure. *J. Chem. Phys.* **2008**, *128*, 182504.

(6) Weckhuysen, B. M. In-situ Characterization of Heterogeneous Catalyst. In *Catalysis, From Principles To Applications*; Beller, M., Renken, A., van Santen, R. A., Eds.; Wiley-VCH: Weinheim, Germany, 2012.

(7) Rodriguez, J. A.; Hanson, J. C.; Chupas, P. J. *In-situ Characterization of Heterogeneous Catalysts*, 1st ed.; John Wiley & Sons: Hoboken, NJ, 2013.

(8) Niemantsverdriet, J. W. Temperature Programmed Techniques. In *Spectroscopy in Catalysis: An Introduction*, 3rd ed.; Wiley-VCH: Weinheim, Germany, 2007.

(9) Ertl, G. Reactions at Surfaces: From Atoms to Complexity. *Angew. Chem., Int. Ed.* **2008**, *47*, 3524−3535.

(10) de Smit, E.; Weckhuysen, B. M. The Renaissance of Iron-Based Fischer−Tropsch Synthesis: On the Multifaceted Catalyst Deactivation Behavior. *Chem. Soc. Rev.* **2008**, *37*, 2758−2781.

(11) Thüne, P. C.; Weststrate, C. J.; Moodley, P.; Saib, A. M.; van de Loosdrecht, J.; Miller, J. T.; Niemantsverdriet, J. W. Studying Fischer−Tropsch Catalysts Using Transmission Electron Microscopy and Model Systems of Nanoparticles on Planar Supports. *Catal. Sci. Technol.* **2011**, *1*, 689−697.

(12) Bozso, F.; Ertl, G.; Grunze, M.; Weiss, M. Chemisorption of Hydrogen on Iron Surfaces. *Appl. Surf. Sci.* **1977**, *1*, 103−119.

(13) Cavalier, J. C.; Chornet, E. Hydrogen-Deuterium Exchange on Iron: Kinetic Anisotropies. *Surf. Sci.* **1976**, *60*, 125−146.

(14) Yoshida, K.; Somorjai, G. A. The Chemisorption of CO, CO_2, C_2H_2, C_2H_4, H_2 and NH_3 on the Clean Fe(100) and (111) Crystal Surfaces. *Surf. Sci.* **1978**, *75*, 46−60.

(15) Imbihl, R.; Behm, R. J.; Christmann, K.; Ertl, G.; Matsushima, T. Phase Transitions of a Two-Dimensional Chemisorbed System: H on Fe(110). *Surf. Sci.* **1982**, *117*, 257−266.

(16) Nichtl-Pecher, W.; Gossman, J.; Hammer, L.; Heinz, K.; Müller, K. Adsorption of Hydrogen on Fe(110) at Cryogenic Temperatures Investigated by Low Energy Electron Diffraction. *J. Vac. Sci. Technol., A* **1992**, *10*, 501−507.

(17) Schmiedl, R.; Nichtl-Pecher, W.; Heinz, K.; Müller, K. Hydrogen on Fe(211): Commensurate and Reconstructed Phases. *Surf. Sci.* **1990**, *235*, 186−196.

(18) Schmiedl, R.; Nichtl-Pecher, W.; Hammer, L.; Heinz, K.; Müller, K. Hydrogen Adsorption on Fe(211): Structural, Thermodynamic and Kinetic Properties. *Surf. Sci.* **1995**, *324*, 289−304.
(19) Merrill, P. B.; Madix, R. J. Hydrogen Bonding on Iron: Correlation of Adsorption and Desorption States on Fe(100) and Perturbation of the Fe-H Bond with Coadsorbed CO. *Surf. Sci.* **1996**, *347*, 249−264.
(20) Suo, H. Y.; Wang, S. G.; Zhang, C. H.; Xu, J.; Wu, B. S.; Yang, Y.; Xiang, H. W.; Li, Y. W. Chemical and Structural Effects of Silica in Iron-Based Fischer−Tropsch Synthesis Catalysts. *J. Catal.* **2012**, *286*, 111−123.
(21) Walch, S. P. Model Studies of the Interaction of H Atoms with bcc Iron. *Surf. Sci.* **1984**, *143*, 188−203.
(22) Sorescu, D. C. First Principles Calculations of the Adsorption and Diffusion of Hydrogen on Fe(100) Surface and in the Bulk. *Catal. Today* **2005**, *105*, 44−65.
(23) van Steen, E.; van Helden, P. A DFT Study of Hydrogen Dissociation on CO- and C-Precovered Fe(100) Surfaces. *J. Phys. Chem. C* **2010**, *114*, 5932−5940.
(24) Jiang, D. E.; Carter, E. A. Adsorption and Diffusion Energetics of Hydrogen Atoms on Fe(110) from First Principles. *Surf. Sci.* **2003**, *547*, 85−98.
(25) Jiang, D. E.; Carter, E. A. Diffusion of Interstitial Hydrogen into and through bcc Fe from First Principles. *Phys. Rev. B* **2004**, *70*, 064102.
(26) Huo, C. F.; Li, Y. W.; Wang, J.; Jiao, H. Surface Structure and Energetics of Hydrogen Adsorption on the Fe(111) Surface. *J. Phys. Chem. B* **2005**, *109*, 14160−14167.
(27) Fabiani, F. C.; Fratesi, G.; Brivio, G. P. Adsorption Of H_2S, HS, S, and H on a Stepped Fe(310) Surface. *Eur. Phys. J. B* **2010**, *78*, 455−460.
(28) Faglioni, F.; Goddard, W. A., III Energetics of Hydrogen Coverage on Group VIII Transition Metal Surfaces and a Kinetic Model for Adsorption/Desorption. *J. Chem. Phys.* **2005**, *122*, 014704.
(29) van Santen, R. A.; Neurock, M. *Molecular Heterogeneous Catalysis: A Conceptual and Computational Approach*; Wiley-VCH: Weinheim, Germany, 2006.
(30) Honkala, K.; Hellman, A.; Remediakis, I. N.; Logadottir, A.; Carlsson, A.; Dahl, S.; Christensen, C. H.; Nørskov, J. K. Ammonia Synthesis from First-Principles Calculations. *Science* **2005**, *307*, 555−558.
(31) Reuter, K.; Scheffler, M. Composition, Structure, and Stability of RuO2(110) as a Function of Oxygen Pressure. *Phys. Rev. B* **2001**, *65*, 035406.
(32) Reuter, K.; Scheffler, M. Composition and Structure of the RuO_2(110) Surface in an O_2 and CO Environment: Implications for the Catalytic Formation of CO_2. *Phys. Rev. B* **2003**, *68*, 045407.
(33) Perdew, J. P.; Burke, K.; Ernzerhof, M. Generalized Gradient Approximation Made Simple. *Phys. Rev. Lett.* **1996**, *77*, 3865−3868.
(34) Blochl, P. E. Projector Augmented-Wave Method. *Phys. Rev. B* **1994**, *50*, 17953−17979.
(35) Kresse, G. From Ultrasoft Pseudopotentials to the Projector Augmented-Wave Method. *Phys. Rev. B* **1999**, *59*, 1758−1775.
(36) Kresse, G.; Furthmüller, J. Efficiency of Ab-initio Total Energy Calculations for Metals and Semiconductors Using a Plane-Wave Basis Set. *Comput. Mater. Sci.* **1996**, *6*, 15−50.
(37) Kresse, G.; Furthmüller, J. Efficient Iterative Schemes for Ab initio Total-Energy Calculations Using a Plane-Wave Basis Set. *Phys. Rev. B* **1996**, *54*, 11169−11186.
(38) Kresse, G.; Hafner, J. First-Principles Study of the Adsorption of Atomic H on Ni (111), (100) and (110). *Surf. Sci.* **2000**, *459*, 287−302.
(39) Methfessel, M.; Paxton, A. T. High-Precision Sampling for Brillouin-zone Integration in Metals. *Phys. Rev. B* **1989**, *40*, 3616−3621.
(40) Jiang, D. E.; Carter, E. A. Carbon Dissolution and Diffusion in Ferrite and Austenite from First Principles. *Phys. Rev. B* **2003**, *67*, 214103.
(41) Sorescu, D. C. First-Principles Calculations of the Adsorption and Hydrogenation Reactions of CH_x (x=0−4) Species on a Fe(100) Surface. *Phys. Rev. B* **2006**, *73*, 155420.
(42) Kittel, C. *Introduction to Solid State Physics*; Wiley: New York, 1996.
(43) Li, W. X.; Stampfl, C.; Scheffler, M. Insights into the Function of Silver as an Oxidation Catalyst by Ab Initio Atomistic Thermodynamics. *Phys. Rev. B* **2003**, *68*, 165412.
(44) Rogal, J.; Reuter, K.; Scheffler, M. Thermodynamic Stability of PdO Surfaces. *Phys. Rev .B* **2004**, *69*, 075421.
(45) Zasada, F.; Piskorz, W.; Cristol, S.; Paul, J. F.; Kotarba, A.; Sojka, Z. Periodic Density Functional Theory and Atomistic Thermodynamic Studies of Cobalt Spinel Nanocrystals in Wet Environment: Molecular Interpretation of Water Adsorption Equilibria. *J. Phys. Chem. C* **2010**, *114*, 22245−22253.
(46) Wang, T.; Liu, X. W.; Wang, S. G.; Huo, C. F.; Li, Y. W.; Wang, J.; Jiao, H. Stability of β-Mo_2C Facets from ab Initio Atomistic Thermodynamics. *J. Phys. Chem. C* **2011**, *115*, 22360−22368.
(47) Wang, T.; Wang, S. G.; Li, Y. W.; Wang, J.; Jiao, H. Adsorption Equilibria of CO Coverage on β-Mo_2C Surfaces. *J. Phys. Chem. C* **2012**, *116*, 6340−6348.
(48) Zhao, S.; Liu, X. W.; Huo, C. F.; Li, Y. W.; Wang, J.; Jiao, H. Surface Morphology of Hägg Iron Carbide (χ-Fe_5C_2) from Ab initio Atomistic Thermodynamics. *J. Catal.* **2012**, *294*, 47−53.
(49) Wang, T.; Tian, X. X.; Li, Y. W.; Wang, J.; Beller, M.; Jiao, H. High Coverage CO Activation Mechanisms on Fe(100) from Computations. *J. Phys. Chem. C* **2014**, *118*, 1095−1101.
(50) Wang, T.; Li, Y.-W.; Wang, J.; Beller, M.; Jiao, H. High Coverage CO Adsorption and Dissociation on the Orthorhombic Mo_2C(100) Surface. *J. Phys. Chem. C* **2014**, *118*, **DOI:** 10.1021/jp412067x.
(51) Frisch, M. J. et al. *Gaussian 09*, revision D.01; Gaussian, Inc.: Wallingford, CT, 2009.
(52) Digne, M.; Sautet, P.; Raybaud, P.; Euzen, P.; Toulhoat, H. Use of DFT to Achieve a Rational Understanding of Acid-Basic Properties of γ-Alumina Surfaces. *J. Catal.* **2004**, *226*, 54−68.
(53) WULFFMAN: An Interactive Crystal Shape Constructor. http://www.ctcms.nist.gov/wulffman/.
(54) Geomview. http://www.geomview.org/.
(55) Huo, C. F.; Wu, B. S.; Gao, P.; Yang, Y.; Li, Y. W.; Jiao, H. The Mechanism of Potassium Promoter: Enhancing the Stability of Active Surfaces. *Angew. Chem., Int. Ed.* **2011**, *50*, 7403−7406.
(56) Spencer, N. D.; Schoonmaker, R. C.; Somorjai, G. A. Iron Single Crystals as Ammonia Synthesis Catalysts: Effect of Surface Structure on Catalyst Activity. *J. Catal.* **1982**, *74*, 129−135.
(57) Koga, K.; Ikeshoji, T.; Sugawara, K. Size- and Temperature-Dependent Structural Transitions in Gold Nanoparticles. *Phys. Rew. Lett.* **2004**, *92*, 115507.
(58) Li, Z. Y.; Yang, N. P.; DiVece, M.; Palmer, S.; Bleloch, A. L.; Curley, B. C.; Johnston, R. L.; Jiang, J.; Yuan, J. Three-Dimensional Atomic-Scale Structure of Size-Selected Gold Nanoclusters. *Nature* **2008**, *451*, 46−48.
(59) van Helden, P.; van den Berg, J. A.; Weststrate, C. J. Hydrogen Adsorption on Co Surfaces: A Density Functional Theory and Temperature Programmed Desorption Study. *ACS Cat.* **2012**, *2*, 1097−1107.
(60) Lynggaard, H.; Andreasen, A.; Stegelmann, C.; Stoltze, P. Analysis of Simple Kinetic Models in Heterogeneous Catalysis. *Prog. Surf. Sci.* **2004**, *77*, 71−137.